2-D Modelling of Dambreak Wave Propagation on Initially Dry Bed

Tawatchai Tingsanchali
Water Engineering and Management Program, School of Civil Engineering,
Asian Institute of Technology, Pathumthani 12120, Thailand

Winyu Rattanapitikon
Department of Civil Engineering, Sirindhorn International Institute of Technology
Thammasat University, Pathumthani 12121, Thailand

Abstract

A 2-D depth-averaged hydrodynamic model is developed to simulate propagation of dambreak wave over an initially dry plane bed under supercritical and subcritical flow conditions. The supercritical flow occurs immediately downstream of the dam due to the discharge through the dambreak section at a very high velocity and a small depth. Further downstream of the dam, the flow is subcritical due to the overriding of the moving surge reflected from the downstream end boundary of the floodplain. The numerical computation is carried out by using an asymmetric finite difference scheme in conjunction with the two-step predictor-corrector MacCormack scheme. The model is applied to simulate the propagation of dambreak wavefront, its spreading pattern and the depth hydrographs in the floodplain considering different floodplain slopes, roughness and reservoir heads. The computed results are compared with the results from the experiments carried out in this study. The agreement is found to be satisfactory. Sensitivity analysis is carried out to determine the individual effects of Manning n, the depth parameters for energy loss calculation and for positioning the wavefront.

1. Introduction

Dams have been built in many parts of the world. Although they were circumspectly designed and constructed, some of them failed. The study of catastrophic flooding after dambreak is of interest because of the risk to life and property in the potentially inundated area below the dam. Though a number of mathematical models of dambreak waves have been developed, these models are mainly one-dimensional (1-D) and only some are two-dimensional (2-D). The 1-D models are suitable for simulating propagation of dambreak waves in a narrow valley or river channel. However, actual flood wave propagation due to dambreak is 2-D and often over dry floodplains. Most of the 2-D models previously developed consider initially wet floodplains and only very few consider initially dry floodplains.

Wattanaprateep [1] developed a 2-D mathematical model of dambreak wave propagation over a dry plane bed. The governing equations are the depth averaged continuity and momentum equations. The asymmetric finite difference scheme [2] with first order accuracy is used to solve the governing equations. The comparison between the experimental and computed results indicated that the model is quite stable but cannot simulate accurately the propagation of dambreak wave which involves both supercritical and subcritical flows. On the other hand, Fennema and Chaudhry [3] applied a two-step predictor-corrector finite difference scheme called the MacCormack scheme [4]with second order accuracy to solve a 2-D propagation of dambreak wave over a plane bed . Their results, although sufficiently accurate, tend to be weakly unstable due to their non-asymmetric nature. To overcome the drawbacks encountered by Wattanaprateep [1] and Fennema and Chaudhry [3], an attempt has been made in this study to develop an accurate 2-D model to compute the propagation of dambreak wave over a dry plane bed.The MacCormack two step predictor-corrector scheme, is combined with asymmetric finite difference scheme, to calculate the propagation of dambreak wave over a dry floodplain which involves both supercritical and subcritical flows. The computed results from the numerical model are verified with the results obtained from the experiments in this study.

2. Mathematical Model

2.1 Governing Equations

The governing equations are the depth averaged two-dimensional continuity equation, x- and y-momentum equations. They can be expressed respectively as follows:

$$\frac{\partial H}{\partial t}+\frac{\partial uh}{\partial x}+\frac{\partial vh}{\partial y}=0 \qquad (1)$$

$$\frac{\partial u}{\partial t}+u\frac{\partial u}{\partial x}+v\frac{\partial u}{\partial y}+g\frac{\partial H}{\partial x}+g\,S_{fx}=0 \qquad (2)$$

$$\frac{\partial v}{\partial t}+u\frac{\partial v}{\partial x}+v\frac{\partial v}{\partial y}+g\frac{\partial H}{\partial y}+g\,S_{fy}=0 \qquad (3)$$

where H is the water level, h is the water depth, u and v are the velocities in x and y directions, t is time, g is the gravitational acceleration, S_{fx} and S_{fy} are the friction slopes in x and y directions.

The friction slopes S_{fx} and S_{fy} are based on the Manning equation in which they can be overestimated when the depth h is approaching zero. To avoid this overestimation, Ramming and Kowalik [5] suggested adding a small depth h_1 to the depth h. The final expression for S_{fx} and S_{fy} becomes:

$$S_{fx}=n^2\,u\,\frac{\sqrt{u^2+v^2}}{(h+h_l)^{4/3}} \qquad (4)$$

$$S_{fy}=n^2\,v\,\frac{\sqrt{u^2+v^2}}{(h+h_l)^{4/3}} \qquad (5)$$

where h_1 is the small depth.

This method is straightforward and is found to work well in most situations without disturbing the accuracy of the model results when the depth is large.

2.2 Numerical Method

To explain the numerical method, it is important to start from the foundation of the asymmetric explicit finite difference scheme. Then the development of the two step predictor-corrector asymmetric finite difference scheme can be explained further as follows:

2.2.1 Asymmetric explicit finite difference scheme [2]

In this scheme, the water level is computed at the center of the meshes while the velocities are computed on the mesh sides as shown in Fig. 1. When $u>0$ or $v>0$, the convective inertia terms $u\frac{\partial u}{\partial x}, v\frac{\partial u}{\partial y}$ in Eq.2 and $u\frac{\partial v}{\partial x}, v\frac{\partial v}{\partial y}$ in Eq.3 are expressed using a backward finite difference scheme. For example,

$$\text{when } u>0, \quad u\frac{\partial u}{\partial x}=u_{i,j}^{k}\,\frac{u_{i,j}^{k}-u_{i-1,j}^{k}}{\Delta x} \qquad (6)$$

On the other hand, a forward finite difference scheme is used when $u<0$ or $v<0$. For example,

$$\text{when } u<0, \quad u\frac{\partial u}{\partial x}=u_{i,j}^{k}\,\frac{u_{i+1,j}^{k}-u_{i,j}^{k}}{\Delta x} \qquad (7)$$

The numerical computation is done as follows:

a) For $u>0$ or $v>0$, the velocities $u_{i,j}^{k+1}$ and $v_{i,j}^{k+1}$ at the time step k+1 are computed from the known values of $u_{i,j}^{k}$, $v_{i,j}^{k}$ and $H_{i,j}^{k}$ at the time k by using the following finite difference equations.

Momentum equation in x-direction

$$u_{i,j}^{k+1}=u_{i,j}^{k}-\frac{\Delta t}{\Delta x}u_{i,j}^{k}\left(u_{i,j}^{k}-u_{i-1,j}^{k}\right)-\frac{\Delta t}{\Delta y}\bar{v}_{i,j}^{k}\left(u_{i,j}^{k}-u_{i,j-1}^{k}\right)-g\frac{\Delta t}{\Delta x}\left(H_{i+1,j}^{k}-H_{i,j}^{k}\right)-g\Delta t\frac{\left[n^2u_{i,j}^{k}\sqrt{\left(u_{i,j}^{k}\right)^2+\left(\bar{v}_{i,j}^{k}\right)^2}\right]}{\left(\overline{hx}_{i,j}^{k}+h_l\right)^{4/3}} \qquad (8)$$

Momentum equation in y-direction

$$v_{i,j}^{k+1} = v_{i,j}^{k} - \frac{\Delta t}{\Delta x}\bar{u}_{i,j}^{k}\left(v_{i,j}^{k} - v_{i-1,j}^{k}\right)$$
$$- \frac{\Delta t}{\Delta y}v_{i,j}^{k}\left(v_{i,j}^{k} - v_{i,j-1}^{k}\right) - g\frac{\Delta t}{\Delta x}\left(H_{i,j+1}^{k} - H_{i,j}^{k}\right)$$
$$- g\Delta t\frac{\left[n^{2}v_{i,j}^{k}\sqrt{\left(\bar{u}_{i,j}^{k}\right)^{2} + \left(v_{i,j}^{k}\right)^{2}}\right]}{\left(\overline{hy}_{i,j}^{k} + h_{l}\right)^{4/3}} \qquad (9)$$

b) The water level $H_{i,j}^{k+1}$ at the time step k+1 is calculated from the known values of $H_{i,j}^{k}$ and the computed velocities $u_{i,j}^{k+1}$ and $v_{i,j}^{k+1}$ from Eqs. 8 and 9 by using the following finite difference continuity equation

Continuity equation

$$H_{i,j}^{k+1} = H_{i,j}^{k} - \frac{\Delta t}{\Delta x}\left[u_{i,j}^{k+1}\overline{hx}_{i,j}^{k} - u_{i-1,j}^{k+1}\overline{hx}_{i-1,j}^{k}\right]$$
$$- \frac{\Delta t}{\Delta y}\left[v_{i,j}^{k+1}\overline{hy}_{i,j}^{k} - v_{i,j-1}^{k+1}\overline{hy}_{i,j-1}^{k}\right] \qquad (10)$$

where

$$\bar{u}_{i,j}^{k} = \left(u_{i,j}^{k} + u_{i,j+1}^{k} + u_{i-1,j+1}^{k} + u_{i-1,j}^{k}\right)/4$$
$$\bar{v}_{i,j}^{k} = \left(v_{i,j}^{k} + v_{i+1,j}^{k} + v_{i+1,j-1}^{k} + v_{i,j-1}^{k}\right)/4$$
$$\overline{hx}_{i,j}^{k} = \left(h_{i,j}^{k} + h_{i+1,j}^{k}\right)/2$$
$$\overline{hy}_{i,j}^{k} = \left(h_{i,j}^{k} + h_{i,j+1}^{k}\right)/2$$

2.2.2 Two-step predictor-corrector asymmetric finite difference scheme

he MacCormack scheme [4] which is a specific type of the two step predictor-corrector finite difference scheme is applied in conjunction with the asymmetric finite difference scheme in solving Eqs. 1, 2 and 3. The computation starts from the predictor step followed by the corrector step. In the predictor step, the predictor values $u_{i,j}^{pk}$, $v_{i,j}^{pk}$, and $H_{i,j}^{pk}$ are determined from the known values of $u_{i,j}^{k}$, $v_{i,j}^{k}$, and $H_{i,j}^{k}$ using Eqs.11 to 13. In the corrector step, the corrector values $u_{i,j}^{ck}$, $v_{i,j}^{ck}$, and $H_{i,j}^{ck}$ are determined from the computed values in the predictor step $u_{i,j}^{pk}$, $v_{i,j}^{pk}$, and $H_{i,j}^{pk}$ using Eqs. 14 to 16. Finally, the values of $u_{i,j}^{k+1}$, $v_{i,j}^{k+1}$, and $H_{i,j}^{k+1}$ are determined by averaging the values at the time step k and the values of the corrector step using Eqs.17 to 19.

The finite difference momentum equations for $u>0$ and $v>0$ and the continuity equation for the predictor step and for the corrector step can be expressed as follows:

a) For predictor step

Momentum equation in x-direction

$$u_{i,j}^{pk} = u_{i,j}^{k} - \frac{\Delta t}{\Delta x}u_{i,j}^{k}\left(u_{i,j}^{k} - u_{i-1,j}^{k}\right)$$
$$- \frac{\Delta t}{\Delta y}\bar{v}_{i,j}^{k}\left(u_{i,j}^{k} - u_{i,j-1}^{k}\right) - g\frac{\Delta t}{\Delta x}\left(H_{i+1,j}^{k} - H_{i,j}^{k}\right)$$
$$- g\Delta t\frac{\left[n^{2}u_{i,j}^{k}\sqrt{\left(u_{i,j}^{k}\right)^{2} + \left(\bar{v}_{i,j}^{k}\right)^{2}}\right]}{\left(\overline{hx}_{i,j}^{k} + h_{l}\right)^{4/3}} \qquad (11)$$

Momentum equation in y-direction

$$v_{i,j}^{pk} = v_{i,j}^{k} - \frac{\Delta t}{\Delta x}\bar{u}_{i,j}^{k}\left(v_{i,j}^{k} - v_{i-1,j}^{k}\right)$$
$$- \frac{\Delta t}{\Delta y}v_{i,j}^{k}\left(v_{i,j}^{k} - v_{i,j-1}^{k}\right) - g\frac{\Delta t}{\Delta x}\left(H_{i,j+1}^{k} - H_{i,j}^{k}\right)$$
$$- g\Delta t\frac{\left[n^{2}v_{i,j}^{k}\sqrt{\left(\bar{u}_{i,j}^{k}\right)^{2} + \left(v_{i,j}^{k}\right)^{2}}\right]}{\left(\overline{hy}_{i,j}^{k} + h_{l}\right)^{4/3}} \qquad (12)$$

Continuity equation

$$H_{i,j}^{pk} = H_{i,j}^{k} - \frac{\Delta t}{\Delta x}\left[u_{i,j}^{pk}\overline{hx}_{i,j}^{k} - u_{i-1,j}^{pk}\overline{hx}_{i-1,j}^{k}\right] - \frac{\Delta t}{\Delta y}\left[v_{i,j}^{pk}\overline{hy}_{i,j}^{k} - v_{i,j-1}^{pk}\overline{hy}_{i,j-1}^{k}\right] \quad (13)$$

b) For corrector step

Momentum equation in x-direction

$$u_{i,j}^{ck} = u_{i,j}^{pk} - \frac{\Delta t}{\Delta x}u_{i,j}^{pk}\left(u_{i+1,j}^{pk} - u_{i,j}^{pk}\right) - \frac{\Delta t}{\Delta y}\bar{v}_{i,j}^{pk}\left(u_{i,j+1}^{pk} - u_{i,j}^{pk}\right) - g\frac{\Delta t}{\Delta x}\left(H_{i+1,j}^{pk} - H_{i,j}^{pk}\right) - g\Delta t\frac{\left[n^2 u_{i,j}^{pk}\sqrt{\left(u_{i,j}^{pk}\right)^2 + \left(\bar{v}_{i,j}^{pk}\right)^2}\right]}{\left(\overline{hx}_{i,j}^{k} + h_l\right)^{4/3}} \quad (14)$$

Momentum equation in y-direction

$$v_{i,j}^{ck} = v_{i,j}^{k} - \frac{\Delta t}{\Delta x}\bar{u}_{i,j}^{pk}\left(v_{i,j}^{pk} - v_{i-1,j}^{pk}\right) - \frac{\Delta t}{\Delta y}v_{i,j}^{pk}\left(v_{i,j}^{pk} - v_{i,j-1}^{pk}\right) - g\frac{\Delta t}{\Delta x}\left(H_{i,j+1}^{pk} - H_{i,j}^{pk}\right) - g\Delta t\frac{\left[n^2 v_{i,j}^{pk}\sqrt{\left(\bar{u}_{i,j}^{pk}\right)^2 + \left(v_{i,j}^{pk}\right)^2}\right]}{\left(\overline{hy}_{i,j}^{k} + h_l\right)^{4/3}} \quad (15)$$

Continuity equation

$$H_{i,j}^{ck} = H_{i,j}^{pk} - \frac{\Delta t}{\Delta x}\left[u_{i,j}^{ck}\overline{hx}_{i,j}^{k} - u_{i-1,j}^{ck}\overline{hx}_{i-1,j}^{k}\right] - \frac{\Delta t}{\Delta y}\left[v_{i,j}^{ck}\overline{hy}_{i,j}^{k} - v_{i,j-1}^{ck}\overline{hy}_{i,j-1}^{k}\right] \quad (16)$$

where

$$\bar{u}_{i,j}^{pk} = \left(u_{i,j}^{pk} + u_{i,j+1}^{pk} + u_{i-1,j+1}^{pk} + u_{i-1,j}^{pk}\right)/4$$

$$\bar{v}_{i,j}^{pk} = \left(v_{i,j}^{pk} + v_{i+1,j}^{pk} + v_{i+1,j-1}^{pk} + v_{i,j-1}^{pk}\right)/4$$

The values at time step $k+1$ are calculated as follows:

$$u_{i,j}^{k+1} = \left(u_{i,j}^{k} + u_{i,j}^{ck}\right)/2 \quad (17)$$

$$v_{i,j}^{k+1} = \left(v_{i,j}^{k} + v_{i,j}^{ck}\right)/2 \quad (18)$$

$$H_{i,j}^{k+1} = \left(H_{i,j}^{k} + H_{i,j}^{ck}\right)/2 \quad (19)$$

2.3 Boundary and Initial Conditions

a) The upstream boundary conditions are the discharge and depth hydrographs at the dambreak section. The downstream boundary conditions are the velocity and depth hydrographs at the downstream outlet. These boundary conditions are obtained from the measurements in the experiments.

b) For the surrounding closed wall boundary, a zero normal velocity is considered. For the tangential velocity along the closed wall, the no-slip boundary condition is assumed, i.e., the velocity tangential to the wall is set equal to zero.

c) The floodplain initial condition is a dry plane bed with $h = 0$, $v = 0$ and $u = 0$. The friction slope S_f is set equal to zero. Computational difficulties as well as diffusion or smearing of the wavefront arise due to very small or occasionally negative depth at boundaries of the flow field. This situation occurs when the grid points with zero depth nearest to the wavefront are considered. To avoid these unfavorable consequences, the computed depth at a newly covered grid is counted only when the depth is larger than a limiting depth of wavefront d_f. The assumed value of $d_f = 0.001h_o$ where h_o is the initial head of the reservoir. In the computation, it is assumed that the flow velocities u and v at the wavefront are equal to the computed velocities nearest to the wavefront in the corresponding directions [6].

2.4 Numerical Stability

To assure the stability of explicit computation, the Courant Stability Criteria is given as follows [2]:

$$\Delta t \le \Delta x\,(-u + \sqrt{u^2 + 0.5gh})\,/gh \quad (20)$$

$$\Delta t \le \Delta y\,(-v + (\sqrt{v^2 + 0.5gh})\,/gh \quad (21)$$

3. Laboratory Experiments

The experimental set up is shown in Fig.2. The reservoir is a tank of 2.8 m long, 1.7 m wide and 0.8 m high. One side of the reservoir is made of a transparent plastic sheet to observe the reservoir water surface profile. A floodplain is made of a wooden plane bed of 4 m long and 1.9 m wide laid downstream of the reservoir and surrounded by transparent vertical walls. The dambreak section is represented by a reservoir gate of 5 cm wide starting from the wooden plane bed to the top of the reservoir tank as shown in Fig.2.

The side walls of the wooden plane are made of transparent plastic sheets to observe the fluctuation of water level over the plane. The downstream end outlet of the wooden plane bed is 0.5 m wide at the center line. The dambreak is simulated by lifting up the gate suddenly by using a falling weight. Slow motion pictures taken by a digital video camera indicate that the gate is suddenly moved upward above the water surface within a time period of less than 0.03 s. Two slopes of floodplain, one horizontal and another 1/200 are considered. For each slope, three initial reservoir heads i.e. 10, 20 and 25 cm above the wooden plane bed are considered.

Measurements of Dambreak Wave Spreading and Depth Hydrographs - The instantaneous outflow through the gate (dambreak section) is determined from the change in reservoir storage volume. By plotting the reservoir water surface profiles with time, the outflow hydrograph through the dambreak section is determined.

For the water depths in the floodplain, staff gage readings are taken by slow motion pictures using a video camera. The depth hydrographs are recorded at 12 positions in the floodplain and 5 positions at the downstream end outflow section.

The instantaneous outflow velocity at the downstream end opening are measured by a 3 mm propeller mini-current meter connected to an automatic recorder.

The propagation of dambreak wavefront is also recorded on slow motion pictures using a video camera at the top of floodplain. Seven hundred and sixty grids each of size 0.1 m x 0.1 m are drawn on the wooden plane bed for tracing the position of the spreading wavefront.

From the experiments, it is observed that water discharges through the dambreak section as a jet spreading two-dimensionally over the plane bed at a small depth and very high velocity until it reaches the downstream end where a rectangular opening and downstream end wall exist. Part of the flow discharges through the opening however, the remaining part of the flow is reflected back by the downstream end wall causing a moving hydraulic jump in the upstream direction. The water level at a station in the floodplain suddenly rises and fluctuates when the moving hydraulic jump arrives and passes over it. This sudden rise and fluctuation of water level is very strong in the region near to the dam where the velocity is high.

4. Numerical Computation

The input data for numerical computation are: 1) Manning roughness coefficient of each grid, 2) surface elevation of the wooden plane, 3) initial dry condition throughout the plane bed, 4) outflow discharge and depth hydrographs through the dambreak section, 5) outflow velocity at the downstream end opening of the plane, 6) the small depth h_1 in the friction slope equations (Eqs.4and 5), h_1 is assumed equal to 0.001 h_o, 7) the limiting depth of wavefront, d_f which is assumed equal to $0.001h_o$, and 8) the distance intervals $\Delta x = \Delta y = 0.1\,\text{m}$ and the time interval $\Delta t = 0.005$ s which satisfy Eqs.20 and 21.

The computed results are the position of leading wavefront in the floodplain, the spreading pattern of wavefront, the depth hydrographs and velocities.

In the numerical computation, three numerical computational procedures have been performed namely: Procedures P1, P2 and P3.

The procedure P1 utilizes the two-step predictor-corrector asymmetric finite difference scheme in both supercritical and subcritical flow regions.

The procedure P2 utilizes only a one step asymmetric finite difference scheme in both flow regions.

The procedure P3 utilizes the procedure P1 in the supercritical flow region, i.e., in the area upstream of the moving hydraulic jump and the procedure P2 in the subcritical flow region, i.e., in the area downstream of the moving hydraulic jump. It is found that the procedure P3 gives the most accurate results compared to the procedures P1 and P2 especially for the water depth hydrographs and takes much less computational time than the procedure P1. Therefore, the procedure P3 is finally selected in this study.

5. Results and Discussions

Typical results of the simulation of propagation of dambreak waves over the dry floodplain with the bed slope $S_o = 0$ and $S_o = 1/200$ and the initial reservoir head $h_o = 0.1\,\text{m}$ are presented. From the calculation, the Manning n of 0.01 is found to give good simulation results. As shown in Figs.3 and 6, it can be seen that the computed position of the leading wavefront agrees closely with the observed data. The experimental results show that the leading wavefront travels from the dam to the downstream end within a time range varying from 4 to 12 s. depending on the initial reservoir head, the floodplain slope and the Manning n. The computed spreading patterns of the wavefront are compared with the observed data as shown in Figs.4 and 7 at various times. The agreement is generally satisfactory. It is noted that the spreading patterns of the wavefront are not symmetrical due to the slightly uneven surface of the floodplain. For the computed depth hydrographs, e.g. at the centerline stations L1, L2 and L4 (distance 0.7, 1.4 m and 3.1m from the dam, respectively), they are compared with the observed data as shown in Figs.5 and 8. The agreement is good except at the time when the moving hydraulic jump crosses over the stations. The difference is due to the error in the computation as well as in the measurements at the jump location. For the numerical simulation of other experimental runs, the same values of parameters are used namely Manning $n = 0.01$, $h_1 = 0.001h_o$ and $d_f = 0.001h_o$. The results are found to be satisfactory. The simulation results when the bed slope $S_o = 1/200$ are better than those when $S_o = 0$.

Sensitivity analysis - A sensitivity analysis of model parameters is carried out to determine the effects of each parameter, i.e., Manning n, the required minimum small depth h_1 for energy loss calculation, the required minimum depth of wavefront computation d_f and the effect of closed wall boundary conditions.

The model computation, the sensitivity of each parameter on the computed results can be described as follows:

1. Manning n - The Manning n is found to have a significant effect on the computed depth hydrograph (Fig.9). Its effect becomes more significant on the position of the leading wavefront and the wavefront spreading pattern (Fig.10). When the Manning n is increased, the computed depth is also increased and the speed of wavefront is decreased. By increasing the Manning n by 3 times from 0.01 to 0.03, the average increase in the depth is about 25% (Fig.9) while the reduction in the speed of the leading wavefront along the center line is about 50% (Fig. 10).

2. The small depth h_1 for energy loss calculation - It is found that when the required minimum depth h_1 in the friction slope equation is increased from its assumed value of $0.001h_o$ (which is about 2% of average flow depth in the supercritical flow region) to $0.01h_o$, the computed water depth in the floodplain is insignificantly changed (Fig. 11). However, a slight change in the computed positions of wavefront and its spreading pattern can be observed (Fig. 12).

3. The limiting depth of wavefront d_f - By changing the limiting depth of wavefront d_f from its assumed value of $0.001h_o$ to $0.01h_o$, there is no detectable difference in the computed depth hydrographs while for the position of leading wavefront and spreading pattern of wavefront, only a slight change can be observed.

4. Effect of closed wall boundary conditions - Though the no-slip wall boundary condition is used for the computation in this study, other types of closed wall boundary conditions are also tried. These are :

a) perfect slip wall boundary condition in which $\partial u/\partial y = 0$ along the wall in x-direction and $\partial v/\partial x = 0$ along the wall in y-direction [7].

b) anti-symmetric reflection boundary condition in which an imaginary point in the solid wall has a velocity parallel to the wall equal to the nearest point in the flow domain but in an opposite flow direction [3].

From the computed water depth hydrographs, it is found that the perfect slip and no-slip boundary conditions yield almost the same result. While the anti-symmetric reflection condition yield larger depths than the perfect slip and no-slip boundary conditions. Therefore, the no-slip boundary condition is finally used.

6. Conclusions

The distance and time steps used in the computation are 0.1 m and 0.005 s respectively. Three types of closed wall boundary conditions are considered namely: no-slip, perfect slip and anti-symmetric reflection. It is found that the no-slip boundary condition gives the most satisfactory results.

The predictor-corrector anti-symmetric finite difference scheme yields good results on the computed propagation of dambreak waves at any station in the supercritical flow region before the arrival of the moving hydraulic jump reflected from the downstream closed walls. After the passage of this reflected jump the flow becomes subcritical, the computational procedure is changed to a one step asymmetric finite difference scheme. The comparison between the computed and measured data for the water depth hydrographs shows a good agreement in general though some discrepancies can be observed when the jump occurs at the centerline station near to the dambreak section where the effect of the reflected moving hydraulic jump is strong. For the comparison of the computed and observed positions of the leading wavefront and the wavefront spreading pattern, the agreement is found to be good. The accuracy of the results may be increased by using a smaller grid size. However, the computation time will be drastically increased.

Sensitivity analysis is carried out to determine the individual effect of Manning n, the small depth h_1 for the friction slope and the limiting depth of wavefront, d_f. It is found that the Manning n has the most significant effect on the computed water depth hydrographs and the propagation of the wavefront.

7. References

[1] Wattanaprateep, T. (1987), Two-Dimensional Propagation of Dambreak Wave, Master Thesis No. WA-85-33, Asian Institute of Technology, Bangkok, Thailand, 129 p.

[2] Zech, Y. (1983), Mathematical Modeling of Floods in Rivers and Uncovering Floodplains, Proceedings, International Conference on Hydraulic Aspects of Flood and Flood Control, London, England, September, pp. 217-227.

[3] Fennema, R.J. and Chaudhry, M.H. (1990), Explicit Methods for 2-D Transient Free-Surface Flows, Journal of Hydraulic Engineering, ASCE, Vol.116, No. 8, August, pp. 1013-1034.

[4] Hirsch, C.H. (1990), Numerical Computation of Internal and External Flows, Volume 1 and 2, John Wiley and Sons, England, pp.243-251.

[5] Ramming, H.G. and Kowalik, Z. (1980), Numerical Modeling of Marine Hydrodynamic-Applications to Dynamic Physical Process, Elsevier Oceanography Series, 368p.

[6] Akanbi, A.A. and Katopodes, N.D. (1988), Model for Flood Propagation on Initially Dry Land, Journal of Hydraulic Engineering, ASCE, Vol. 114, No. 7, July, pp. 689-760.

[7] Ponce, V.M. and Yabusaki, S.S. (1980), Mathematical Modeling of Circulation in Two-Dimensional Plane Flow, Final Report for the National Sciences Foundation, Colorado State University, Fort Collins, Colorado, U.S.A., 289 p.

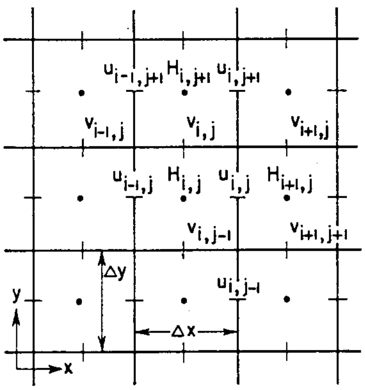

Fig. 1 Diagram of 2-D Grid System

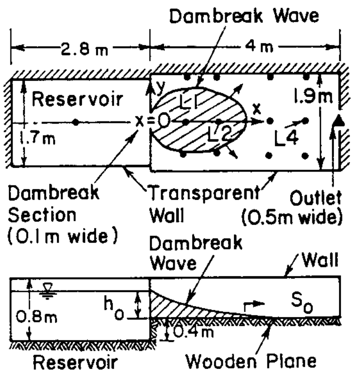

Legend : • Depth Gaging Station
▲ Velocity Gaging Station

Fig. 2 Experimental Setup

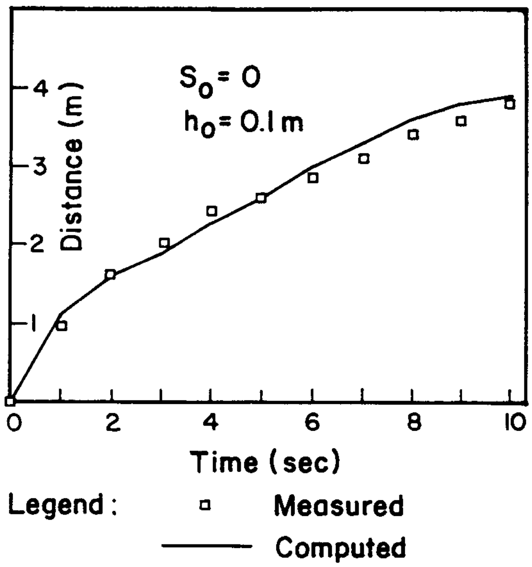

Fig. 3 Measured and Computed Paths of Wavefront

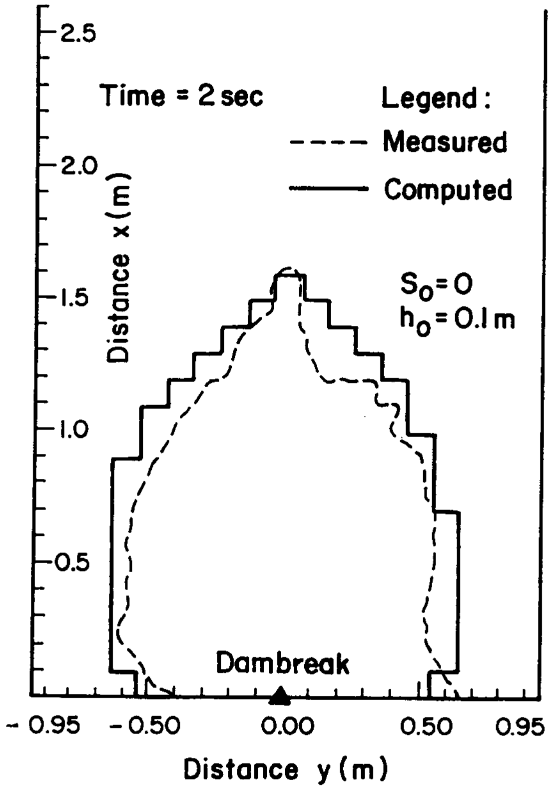

Fig. 4 Measured and Computed Wavefront Propagation

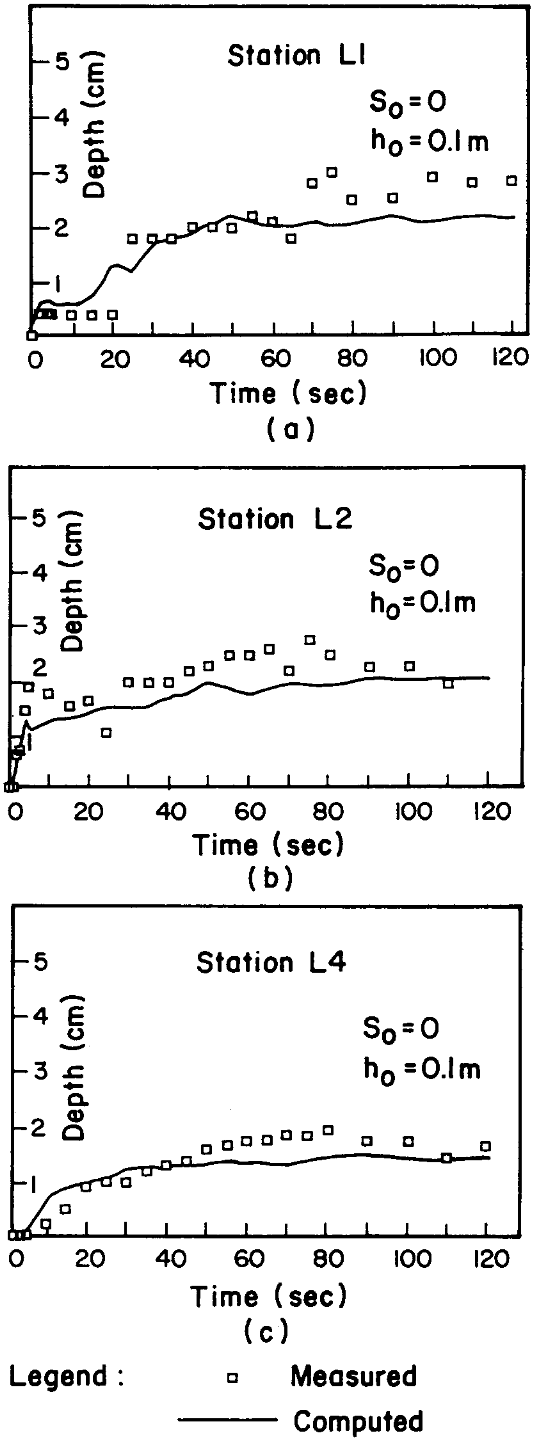

Fig. 5 Measured and Computed Depth Hydrographs at Stations L1, L2 and L4

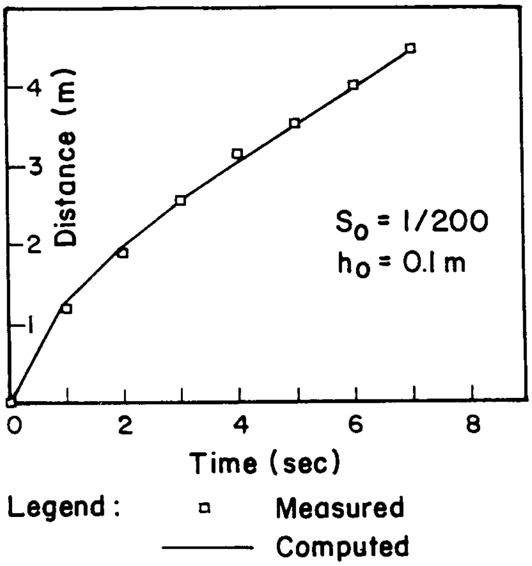

Fig. 6 Measured and Computed Paths of Wavefront

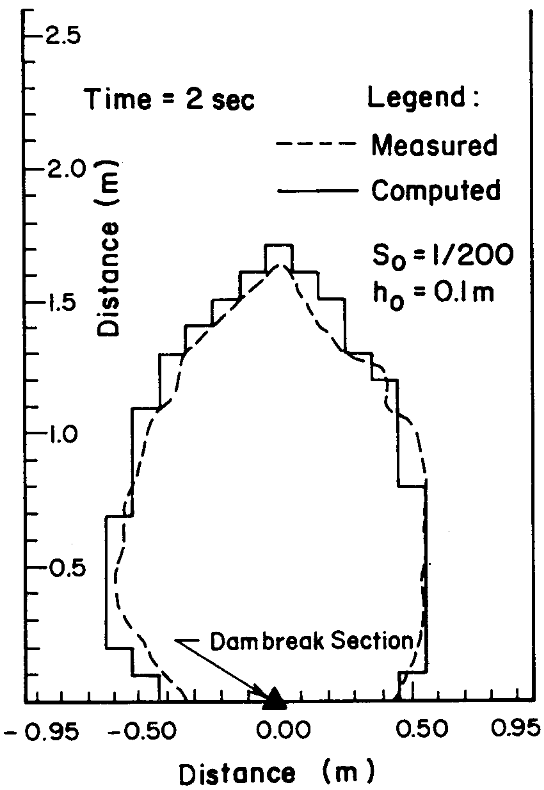

Fig. 7 Measured and Computed Wavefront Propagation

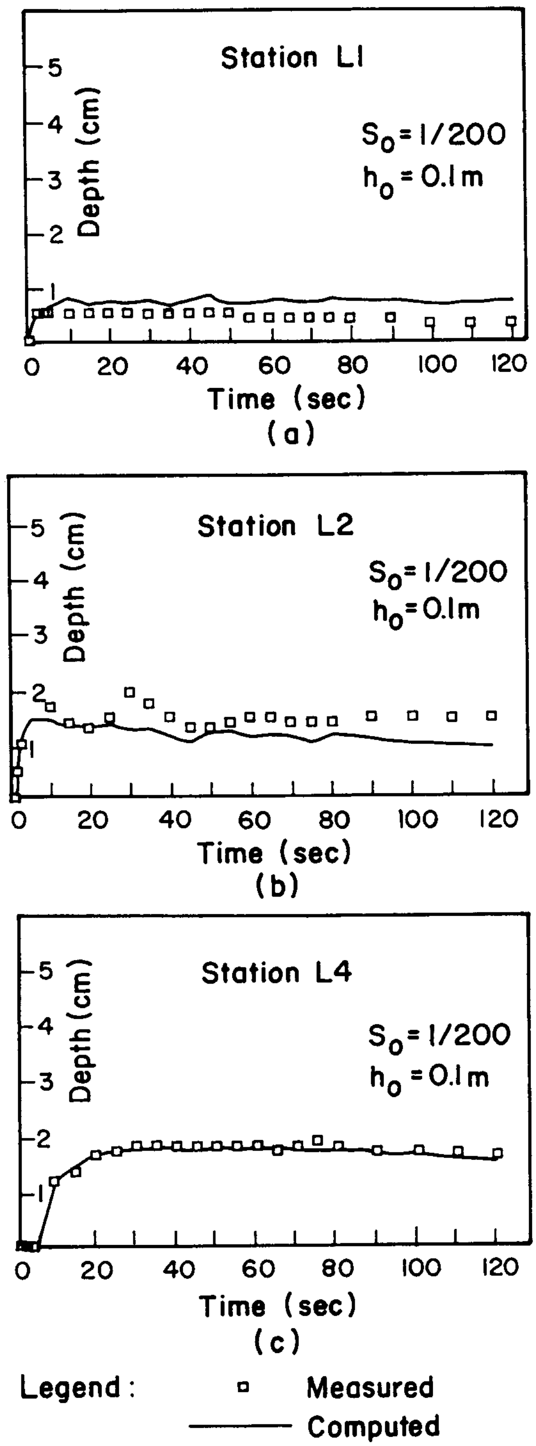

Fig. 8 Measured and Computed Depth Hydrographs at Stations L1, L2 and L4

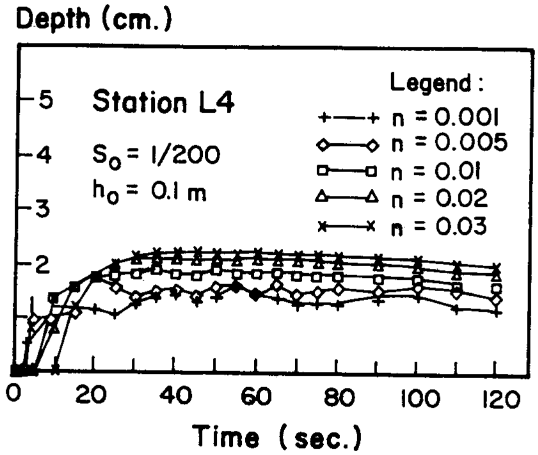

Fig. 9 Effects of Manning n on Depth Hydrographs

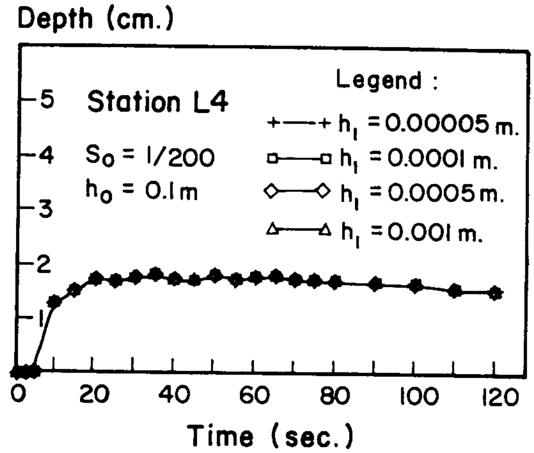

Fig. 11 Effects of Small Depth h_l on Depth Hydrographs

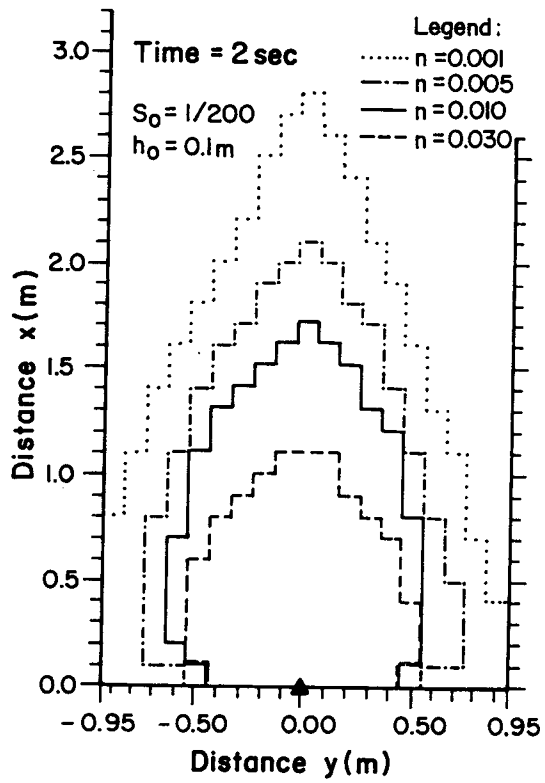

Fig. 10 Effects of Manning n on Wavefront Propagation

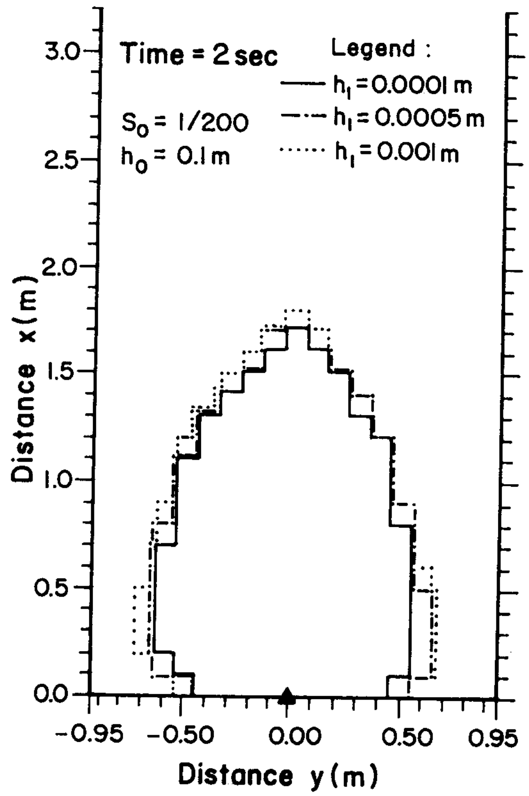

Fig. 12 Effects of Small Depth h_l on Wavefront Propagation